

FEATURE ARTICLE

Sum Frequency Generation from Langmuir–Blodgett Multilayer Films on Metal and Dielectric Substrates

Jasper Holman and Paul B. Davies*

Department of Chemistry, University of Cambridge, Lensfield Road, Cambridge, CB2 1EW, UK

Takuma Nishida and Shen Ye*

Catalysis Research Center, Hokkaido University, Sapporo 001-0021, Japan

David J. Neivandt

*Department of Chemical and Biological Engineering, University of Maine, Orono, Maine 04469**Received: March 28, 2005; In Final Form: July 7, 2005*

Sum frequency generation (SFG) vibrational spectra of cadmium arachidate multilayer films adsorbed on a substrate with high nonresonant susceptibility, i.e., gold, and on a low nonresonant susceptibility substrate, i.e., fused quartz, have been investigated in the C–H stretching region in air. The films were formed by Langmuir–Blodgett (LB) deposition and their spectra recorded using SFG spectrometers employing both 532-nm nanosecond and 800-nm femtosecond lasers, with counter-propagating and co-propagating beam geometries, respectively. Both kinds of substrate were rendered hydrophobic by coating them with per-deuterated octadecanethiol (gold) or per-deuterated cadmium arachidate (fused quartz) monolayers. Single per-protonated arachidate layers in otherwise per-deuterated 10-layer films were used to show that the SFG resonances arise only from the topmost and lowermost layers in a LB film comprised of an even number of per-protonated layers, although the SFG spectra from the two hydrophobic substrates are different from each other. The differences in the spectra from the same ten-layer per-protonated films deposited on the two types of hydrophobic substrate have been explained in terms of a simple model that accounts for resonant and nonresonant contributions.

Introduction

Organic multilayer structures have many applications in biology, chemistry, and physics.¹ Lipid multilayers on solid substrates provide a convenient way of studying biomimetic systems,² while fatty acid multilayers are strong candidates for incorporation into molecular electronic devices, photovoltaic devices and nonlinear materials.³ A versatile way of creating these multilayer structures is by Langmuir–Blodgett (LB) deposition.⁴ The LB technique not only allows precise control of the molecular structure within the deposited multilayer, but also of the film thickness, which is determined by the length and orientation of the molecules comprising the layer.

LB multilayer films comprising fatty acids have been studied by a variety of techniques such as optical absorbance,⁵ grazing incidence X-ray diffraction (GIXD),⁶ electron diffraction,⁷ neutron diffraction,⁸ and atomic force microscopy (AFM).⁹ The consensus of such studies is that LB films of the cadmium salts of fatty acids longer than dodecyl consist of highly ordered domains of alkyl chains in near perfect trans conformations and further, that the alkyl chains of the fatty acids are oriented in a

plane perpendicular to the film surface, with the cadmium cations located between the fatty acid layers. Deposition of fatty acid films onto solid substrates at neutral pH results almost exclusively in a Y-type morphology, i.e., head-to-head and tail-to-tail, perpendicular to the surface. The amphiphilic nature of fatty acids results in different preferred structures on hydrophilic and hydrophobic substrates. Thus, fatty acid multilayer films deposited on hydrophobic substrates in air consist of an even number of individual layers with the lowermost layer oriented with its hydrophobic alkyl chain pointing toward the substrate and the topmost layer oriented with its alkyl chain away from the substrate into air. Conversely, fatty acid multilayer films deposited on hydrophilic substrates in air consist of an odd number of individual layers, with the lowermost layer oriented with its hydrophobic alkyl chain away from the substrate. The topmost layer is, in common with films on hydrophobic substrates, oriented with its alkyl chains away from the substrate into air.

The second-order nonlinear optical technique of sum frequency generation (SFG) vibrational spectroscopy is a powerful tool for studying adsorption and reaction at interfaces due to the detailed molecular orientation and conformational information that it can provide.¹⁰ SFG is achieved via the spatial and

* Corresponding authors. Davies: Tel +44 1223 336460; fax: +44 1223 336362; e-mail pbd2@cam.ac.uk. Ye: Tel +81 11 706 9126; fax: +81 11 706 9124; e-mail ye@cat.hokudai.ac.jp.

Jasper Holman received his M.Sc. (cum laude) from the University of Groningen in 2001, which included three months at the University of Liverpool on an Erasmus studentship of the European Community. He carried out his Ph.D. research in sum frequency spectroscopy at the University of Cambridge from 2001 to 2004, holding an Oppenheimer Fund studentship. During the spring of 2004, he held a Japan Society for the Promotion of Science (JSPS) Fellowship at Hokkaido University. In September 2004, he joined the graduate program at BP.

Paul B. Davies graduated from the University of Liverpool (B.Sc. 1964) and received his Ph.D. from the University of Cambridge in 1968. After spending a year as a postdoctoral fellow at Harvard University, he returned to the chemistry department at Cambridge and has been on the academic staff there since 1972. His research interests encompass several aspects of infrared laser spectroscopy, including high-resolution mid and far infrared spectroscopy of transient species in the gas phase and the structure of interfacial adsorbates studied using primarily sum frequency generation spectroscopy. He has extensive collaborative programs on these topics in Japan, Germany, and the United States.

Takuma Nishida obtained his B.S. degree in 2002 from the Department of Chemistry, and his M.S. degree in 2004 from the Graduate School of Environmental Earth Science, Hokkaido University, Japan. He is now a Ph.D. student. His research interests include the study of nonlinear vibrational spectroscopy, self-assembled monolayers (SAMs), and Langmuir–Blodgett (LB) films.

Shen Ye graduated from the Ocean University of China in 1986 and received his Ph.D. degree in 1993 from Hokkaido University, Japan. He started his nonlinear optical studies on solid surfaces as a research fellow in the Department of Physics, University of California at Berkeley in 1997. He was a PRESTO researcher, Japan Science and Technology Corporation (JST) from 2000 to 2003. He has been on the faculty of the Department of Chemistry, Hokkaido University since 1993, and in 2001 became an associate professor in the Catalysis Research Center, Hokkaido University. His research interests include the study of surface electrochemistry, organic thin films including SAMs, LB films, polymers, and lipid bilayers, in situ vibrational spectroscopy, and nonlinear optics.

David J. Neivandt received his B.Sc. (1994) and Ph.D. (1998) in Chemistry, with a focus in colloid and interface science, from the University of Melbourne. He was subsequently appointed an Oppenheimer Research Fellow at the University of Cambridge. From 2001 he has been an Assistant Professor in the Department of Chemical and Biological Engineering at the University of Maine. His research interests are in the study of adsorption from polymer and surfactant solutions, and their mixtures, on industrially relevant surfaces, and the study of lipid membrane structure as a function of protein adsorption and transport processes.

temporal overlap of a fixed frequency visible or near-infrared laser beam and a tunable frequency infrared laser beam on an interface. A third beam, with a frequency equal to the sum of the two incident laser frequencies (the SF beam) is emitted from the interface. Measuring the intensity of the emitted SF light as the infrared frequency is scanned over a vibrational mode or modes produces a vibrational spectrum of the interfacial species. The symmetry-based selection rules for SFG make the technique inherently interface specific. Additionally, SFG is sensitive to submonolayer surface coverage and may be applied under ambient conditions. Due to the unique way in which SFG probes the interfacial layer it often provides complementary information to other surface techniques. Both metallic and dielectric substrates have been used in SFG measurements of adsorbates at the solid/air and solid/liquid interfaces. The use of metallic substrates such as gold and silver results in the effective enhancement of the SFG signal arising from the adsorbate due to the large nonresonant susceptibility of these metals. An important consequence of the SFG signal arising from the metal as well as from the molecular adsorbate is that it allows the

facile determination of the polar orientation of the adsorbate from the spectral phase of the resonances, i.e., positive (peaks) or negative (dips).^{11,12}

Two different types of infrared laser sources are employed in SFG spectrometers, narrowband and broadband.^{13,14} Usually, in narrowband spectrometers, a narrow line width infrared laser is scanned in frequency across the region of interest under the excitation of a near-infrared or visible pulse at the wavelength of the fundamental (1064-nm) or second harmonic output (532-nm) of a nanosecond or picosecond Nd:YAG laser. Conversely, in broadband spectrometers, a wide line width infrared source (typically $\approx 200 \text{ cm}^{-1}$) and a narrow-band near-infrared pulse at the fundamental (800-nm) of a femtosecond Ti:sapphire laser are employed and the entire spectrum is collected simultaneously exploiting the multiplex advantage.¹⁵ The SFG technique has been applied to a substantial number of experimental systems including biomembranes,^{16–18} polymer films,^{19–21} and fatty acid LB multilayer films.^{22–25} Since LB films have been extensively investigated and characterized by other techniques over many years, they constitute model systems for understanding SFG from multilayer structures. Recent SFG studies of LB films of the cadmium salts of fatty acids have highlighted differences between films formed on different substrates and investigated by different laser systems.

Using a broadband femtosecond laser system with an excitation wavelength of 800-nm, Ye et al.^{22,25} found that SFG spectra from multilayers of cadmium stearate adsorbed on hydrophilic gold and fused quartz in air were virtually independent of layer thickness. This finding was interpreted in terms of SFG activity solely of the topmost layer, consistent with the interface specificity of SFG. The SFG active layer was found to be highly conformationally ordered and to have the methyl groups of the aliphatic chains oriented into air. Employing a narrowband nanosecond spectrometer with an excitation wavelength of 532-nm to investigate multilayer cadmium salt fatty acid films on hydrophobic gold, Holman et al.²³ confirmed the presence of hydrocarbon chains in an *all-trans* conformation. However, in contrast with the conclusion of Ye et al., it was found that the SFG signal arose from both the topmost and lowermost fatty acid layers and that the observed signal was in fact a summation of the individual spectra of these two layers, but with the topmost layer making the larger contribution. The spectra were found to be further characterized by the presence of a thin film thickness interference effect that affected the line shape of the asymmetric methyl stretching mode, a finding that in itself is qualitative confirmation that one of the two layers is separated from the substrate by changing distances as the film thickness is varied by altering the number of layers. This thickness dependent interference effect was quantified in a subsequent article²⁶ using the theory that describes thickness dependent interference in SFG spectra developed by Lambert et al.²⁷ In contrast, the film thickness interference effect was not observed in the SFG spectra of fatty acid multilayer films with a maximum thickness of 12-layers when deposited on hydrophilic gold or fused quartz substrates recorded on the femtosecond (800-nm) spectrometer of Ye et al.^{22,25}

In the present work, we show that it is possible to rationalize the differences between spectra recorded from multilayers on different substrates with two spectrometers operating at different wavelengths and with different optical geometries, thereby providing a deeper understanding of the phenomenon of SFG from multilayer structures. SFG spectra of multilayers composed of cadmium arachidate deposited onto per-deuterated octadecanethiol (d-ODT) coated gold substrates, i.e., hydrophobic gold,

and onto fused quartz coated with a single layer of per-deuterated cadmium arachidate, i.e., hydrophobic fused quartz, have been recorded in the aliphatic C–H stretching region (2800–3000 cm⁻¹). Selective per-deuteration/per-protonation of specific layers within the cadmium arachidate multilayer structures has been employed to further elucidate the origin of the SFG signal. The experimental results are interpreted in terms of a simple and unified theoretical framework.

Theory

The successful interpretation of the resonant intensities and spectroscopic phases of the multilayer SFG spectra recorded here and previously can be achieved by consideration of the similarities and differences in spectral features of four different systems: first, the differences that occur between spectra recorded on metal and dielectric substrates; second, differences in the laser systems and optical beam geometries used; third, optical interference effects from thin films deposited onto different substrates; and last, differences between hydrophilic and hydrophobic surfaces. To achieve a quantitative understanding we begin by consideration of the most fundamental system. Specifically, a resonantly active monolayer (or submonolayer), such as an adsorbed fatty acid film, on a substrate with significant nonresonant SFG activity such as gold or silver, or on a substrate with weak nonresonant SFG activity such as fused quartz or calcium fluoride (CaF₂). The SFG intensity (I_{SFG}) can be envisaged as a combination of a resonant susceptibility contribution ($\chi_{\text{R}}^{(2)}$) arising from the molecular layer and a nonresonant susceptibility contribution ($\chi_{\text{NR}}^{(2)}$) arising from the substrate,

$$I_{\text{SFG}} \propto |\chi_{\text{R}}^{(2)} + \chi_{\text{NR}}^{(2)}|^2 \quad (1)$$

which can be expanded to include the resonant (δ) and nonresonant (ϵ) phases:

$$\begin{aligned} I_{\text{SFG}} &\propto |\chi_{\text{R},ijk}^{(2)} e^{i\delta} + \chi_{\text{NR},ijk}^{(2)} e^{i\epsilon}|^2 \\ &= \{|\chi_{\text{R},ijk}^{(2)}| e^{i\delta} + |\chi_{\text{NR},ijk}^{(2)}| e^{i\epsilon}\} \times \{|\chi_{\text{R},ijk}^{(2)}| e^{i\delta} + |\chi_{\text{NR},ijk}^{(2)}| e^{i\epsilon}\}^* \\ &= |\chi_{\text{R},ijk}^{(2)}|^2 + |\chi_{\text{NR},ijk}^{(2)}|^2 + 2|\chi_{\text{R},ijk}^{(2)}||\chi_{\text{NR},ijk}^{(2)}|\cos[\epsilon - \delta] \quad (2) \end{aligned}$$

where i , j , and k represent the tensor components of $\chi^{(2)}$ in the laboratory frame and * represents the complex conjugate.

It is instructive to consider how the relative magnitudes of the terms on the right-hand side of eq 2 are dependent on the nature of the substrate. Where the substrate is a dielectric $\chi_{\text{R}}^{(2)} \gg \chi_{\text{NR}}^{(2)} \approx 0$ and eq 2 reduces to the first squared term only. As a consequence, SFG spectra of a monolayer on fused quartz are invariably peak shaped. Conversely, for a metal substrate such as gold, $\chi_{\text{NR}}^{(2)}$ is dependent on the excitation wavelength and typically is comparable in magnitude to $\chi_{\text{R}}^{(2)}$.^{28–31} Contributions from all terms of eq 2 must therefore be considered. The $\chi_{\text{NR}}^{(2)}$ term is (typically) almost constant with infrared frequency and hence provides a nearly frequency independent background SFG signal. The third term in eq 2, a cross term of the resonant and nonresonant susceptibilities, containing the phase angles, provides a second resonant contribution to the SFG spectrum.

The line shapes of the spectral features appearing in an SFG spectrum are determined by the relationship between the phase angles δ and ϵ , provided there is a strong nonresonant background. The nonresonant phase angle ϵ can be considered to be infrared frequency independent over the measured

frequency range. On a gold substrate, its value is approximately +90° for the counter propagating beam geometry of the nanosecond spectrometer with an excitation wavelength of 532 nm.^{28,29} The absolute value of these phases is dependent upon the precise geometry, wavelength, and the polarization combination employed.^{28–31} The resonant phase δ varies as the infrared frequency tunes through the resonant frequency of a specific vibrational mode and can be modeled with a phase angle of $\delta = +90^\circ$ on resonance if this mode is located in a functional group oriented in a direction away from the interface.³² For present purposes the symmetric (r^+) and asymmetric (r^-) stretching modes of the methyl group are assumed to have the same phase. Thus, the counter-propagating geometry using 532-nm visible light will lead to constructive interference between the resonant and nonresonant phases ($\cos(\epsilon - \delta) = 1$ in eq 2), giving rise to spectral resonances of positive phase, i.e., peaks. Conversely, if the resonant functional group is oriented toward the surface, the spectral features appear with negative phase i.e., as dips, due to destructive interference.

The opposite of these situations occurs when a co-propagating geometry is employed. It is known that for the PPP (sum frequency, visible, infrared) beam polarization combination contributions are made by four susceptibility components; $\chi_{\text{zzz}}^{(2)}$, $\chi_{\text{xzx}}^{(2)}$, $\chi_{\text{zxx}}^{(2)}$ and $\chi_{\text{zxx}}^{(2)}$. As previously discussed by Hines et al.,³⁰ although the Fresnel factors corresponding to $\chi_{\text{zzz}}^{(2)}$ and $\chi_{\text{xzx}}^{(2)}$ (specifically those with polarization of the infrared laser beam in the z direction, the dominant molecular orientation) have the same sign in both geometries, $\chi_{\text{xzx}}^{(2)}$ and $\chi_{\text{zxx}}^{(2)}$ (the dominant substrate contributions) have reversed signs and consequently on gold surfaces the counter-propagating geometry produces reversed spectral features relative to the co-propagating geometry. In addition to geometrical contributions to spectral phases, the visible/near-infrared excitation wavelength has a significant effect due to potential correspondence with interband transitions of gold.^{29,31} Nevertheless, for both spectrometers the orientation of the functional group with respect to the surface defines the phase of the resonant SFG signal and consequently the orientation of the resonant group can be deduced from the phase of the signal. We have confirmed that the different visible wavelengths of the two spectrometers does not affect the validity of the orientational conclusions by recording the SFG spectrum of a monolayer of ODT on gold in the PPP polarization combination using a co-propagating geometry, and visible wavelengths of 532 and 800 nm. Both spectra were closely similar, with the resonances appearing with negative phase, i.e., dips. This result is directly applicable when the resonant and nonresonant contributions to the SFG signal are not spatially separated. In cases where different sources of SFG are spatially separated from each other, the model can be extended by including a propagation distance term in the phase factor. This development accounts for thickness dependent interference effects in SFG spectra and has been described in detail by Lambert et al.²⁷ However, it should be noted that on dielectric substrates (with insignificant nonresonant susceptibilities) the SSP beam polarization combination that probes solely the $\chi_{\text{yyz}}^{(2)}$ component is typically employed. Following the discussion above, it is expected, and indeed observed, that resonances of positive phase (peaks) occur on dielectric substrates irrespective of the beam geometry.

The model for the SFG intensities, given in eqs 1 and 2, can be expanded to include a second resonant SFG active layer, specifically a layer that is spatially removed normal to the substrate. This model would be appropriate for example for representing a multilayer film in which only the topmost and

lowermost layers were resonantly SFG active. The observed SFG signal may then be described by expanding eq 1,

$$I_{\text{SFG}} \propto |\chi_{\text{top}}^{(2)} + \chi_{\text{lower}}^{(2)} + \chi_{\text{NR}}^{(2)}|^2 \\ = (\chi_{\text{top}}^{(2)} + \chi_{\text{lower}}^{(2)} + \chi_{\text{NR}}^{(2)}) \times (\chi_{\text{top}}^{(2)*} + \chi_{\text{lower}}^{(2)*} + \chi_{\text{NR}}^{(2)*}) \quad (3)$$

where $\chi_{\text{top}}^{(2)}$ and $\chi_{\text{lower}}^{(2)}$ are the resonant susceptibilities of the two layers. Expanding eq 3 gives

$$= |\chi_{\text{top}}^{(2)}|^2 + |\chi_{\text{lower}}^{(2)}|^2 + |\chi_{\text{NR}}^{(2)}|^2 + \chi_{\text{top}}^{(2)} \chi_{\text{lower}}^{(2)*} + \chi_{\text{top}}^{(2)} \chi_{\text{NR}}^{(2)*} + \\ \chi_{\text{lower}}^{(2)} \chi_{\text{top}}^{(2)*} + \chi_{\text{lower}}^{(2)} \chi_{\text{NR}}^{(2)*} + \chi_{\text{NR}}^{(2)} \chi_{\text{top}}^{(2)*} + \chi_{\text{NR}}^{(2)} \chi_{\text{lower}}^{(2)*} \quad (4)$$

which rearranges to

$$I_{\text{SFG}} \propto |\chi_{\text{top}}^{(2)} + \chi_{\text{NR}}^{(2)}|^2 + |\chi_{\text{lower}}^{(2)} + \chi_{\text{NR}}^{(2)}|^2 + \chi_{\text{top}}^{(2)} \chi_{\text{lower}}^{(2)*} + \\ \chi_{\text{lower}}^{(2)} \chi_{\text{top}}^{(2)*} - |\chi_{\text{NR}}^{(2)}|^2 \quad (5)$$

Equation 5 provides a general mathematical description of SFG arising from two different resonant SFG active layers and a nonresonant SFG active substrate. It is now useful to revisit the two limiting cases, which were considered earlier for a single resonant layer on a substrate with weak or strong nonresonant signal, with regards to eq 5. First, SFG from a system in which the substrate makes a very weak nonresonant contribution to SFG such as when fused quartz, CaF_2 or mica, are employed. Second, the case in which a relatively strong nonresonant background arises from the substrate (such as when gold or silver is employed) which is comparable to that of the resonant signals.^{28–31} In the first case, with $\chi_{\text{NR}}^{(2)} \gg \chi_{\text{NR}}^{(2)*} \approx 0$, eq 5 reduces to,

$$I_{\text{SFG}} \propto |\chi_{\text{top}}^{(2)}|^2 + |\chi_{\text{lower}}^{(2)}|^2 + \chi_{\text{top}}^{(2)} \chi_{\text{lower}}^{(2)*} + \chi_{\text{lower}}^{(2)} \chi_{\text{top}}^{(2)*} \quad (6)$$

whereas $|\chi_{\text{top}}^{(2)}|^2$ and $|\chi_{\text{lower}}^{(2)}|^2$ are real, $\chi_{\text{top}}^{(2)}$ and $\chi_{\text{lower}}^{(2)}$ are complex quantities that may be determined by fitting the experimental SFG data to a set of generic susceptibilities for individual modes (q) given by

$$\chi_{\text{R}}^{(2)} = \sum_q \frac{A_q}{\omega_{\text{IR}} - \omega_{v,q} + i\Gamma_q} \quad (7)$$

where $\omega_{v,q}$, A_q , and Γ_q are the frequency, strength, and damping factor respectively of the q th vibrational mode and ω_{IR} is the infrared laser frequency.³² As indicated in eq 6, the SFG intensity of the system is contributed to by the summation of two individual spectra ($|\chi_{\text{top}}^{(2)}|^2$ and $|\chi_{\text{lower}}^{(2)}|^2$) as well as by the cross terms given by the third and fourth terms in the equation.

For the second case, where a metal substrate such as gold or silver is employed, $|\chi_{\text{NR}}^{(2)}|$ is comparable to $|\chi_{\text{NR}}^{(2)*}|$.^{28–31} Assuming that $\chi_{\text{NR}}^{(2)}$ is a constant in the SFG spectral region of interest then,

$$I_{\text{SFG}} \propto |\chi_{\text{top}}^{(2)} + \chi_{\text{NR}}^{(2)}|^2 + |\chi_{\text{lower}}^{(2)} + \chi_{\text{NR}}^{(2)}|^2 + \chi_{\text{top}}^{(2)} \chi_{\text{lower}}^{(2)*} + \\ \chi_{\text{lower}}^{(2)} \chi_{\text{top}}^{(2)*} - |\chi_{\text{NR}}^{(2)}|^2 \quad (8)$$

Procedures similar to those described for eq 6 are necessary to analyze the resulting SFG spectra. As will be discussed in the Results and Discussion section, however, contributions from

the third and fourth terms on the right-hand side of eq 8 are much smaller than those of the first and second terms.

Experimental Section

Monolayers of cadmium arachidate were prepared at the subphase/air interface by spreading chloroform solutions of the arachidic acid (1.00 mg/mL) onto a LB trough (FSD-500, USI) containing a subphase of cadmium chloride (0.2 mM) and sodium hydrocarbonate (0.3 mM) in 18.2 M Ω cm Milli-Q water, (pH \sim 6.6). Surface pressures were measured using Wilhelmy plates of Whatman Chr1 paper. Following chloroform evaporation, films were compressed to a surface pressure of 30 mN/m and allowed to equilibrate for 30 min. LB layers were deposited by sequential dipping either onto a silicon wafer coated with a hydrophobic gold layer or onto the bottom of a hemicylindrical fused quartz prism (IR grade, $d = 25$ mm, $l = 25$ mm), by vertical and horizontal dipping, respectively.²⁵ Films incorporating combinations of per-deuterated and per-protonated fatty acid layers were formed by the procedure outlined above with the exception that the spread film was changed from per-protonated to per-deuterated fatty acid, or vice-versa, at the requisite time. Complete removal of the old film from the subphase/air interface was verified by the recording of a flat π -A isotherm prior to the spreading of the new layer. Transfer ratios were, within error, unity for all deposited layers.

The hydrophobic gold substrates employed were formed by self-assembly of per-deuterated octadecanethiol (d-ODT) films from methanolic (HPLC grade) solutions onto 150 nm thick gold layers thermally evaporated onto chromium primed polished silicon wafers. Solubilization of d-ODT in methanol was achieved by sonication of a needle tip quantity at 40 °C for 30 min. The gold coated silicon wafers were subsequently immersed in the d-ODT methanol solution for 12 h at ambient temperature to facilitate self-assembly of a d-ODT monolayer. The fused quartz prisms were rendered hydrophilic by sonicating them in acetone followed by immersion in a boiling sulfuric acid/nitric acid mixture, and finally extensive rinsing with Milli-Q water. All chemicals were used as received and obtained from Aldrich with the exception of the per-deuterated arachidic acid, which was obtained from CDN Isotopes, and the d-ODT, which was supplied by Dr. R. K. Thomas, University of Oxford.

SFG spectra were recorded in the C–H stretching region (2800–3000 cm^{-1}). The nanosecond spectrometer has been described elsewhere.³³ In brief, a frequency doubled Nd:YAG laser provides 532 nm light (9 ns, 3 mJ, 11 Hz). About 10% of the 532 nm beam is used as the visible radiation for the SFG experiment. The remainder is used to pump a dye laser, generating red light, which is subsequently Stokes shifted into the infrared by stimulated Raman scattering (third Stokes shift) from a cell containing 36 atm of hydrogen. The broadband femto-second laser spectrometer²² is built from a Ti:sapphire femto-second oscillator/regenerative amplifier laser system (Hurricane, Spectra Physics, 80 fsec, 1 mJ, 800 nm, 1 kHz). About 80% of the laser output was used to pump an optical parametric amplifier (OPA) system (TOPAS, Light Conversion Inc.) to generate a broadband tunable IR beam (200 cm^{-1}). The remainder of the broadband visible output at 800 nm was narrowed to a line width of 10 cm^{-1} by passing it through a Spectral Shaper (TII, Tokyo). The visible and infrared beams were overlapped on the substrate with incident angles of 65° and 50° respectively, and powers of 2 μ J using a co-propagating beam geometry. The SFG signal was dispersed through a monochromator (MS350 li, Solar-TII) and collected with a CCD camera (DU420–BV, Andor Technology). When fused quartz

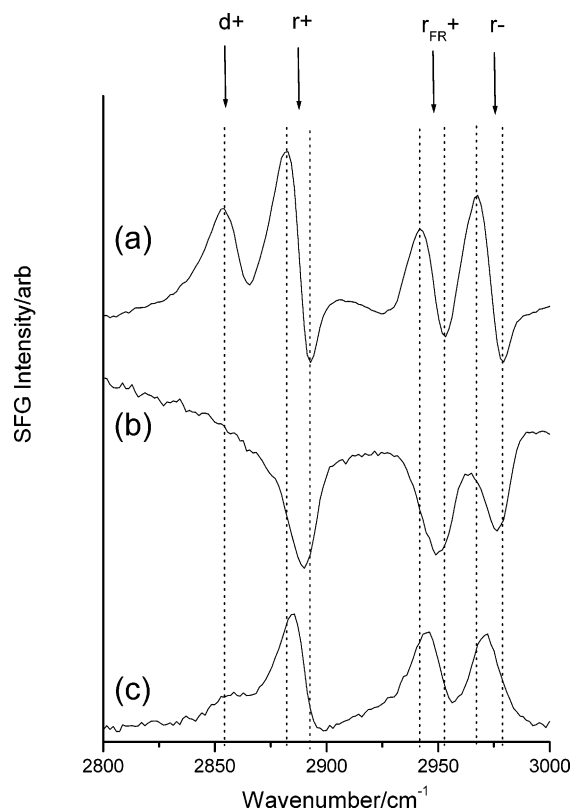


Figure 1. The 800-nm excited broadband SFG spectra of: (a) ten layer per-protonated cadmium arachidate multilayer film, (b) nine layer per-deuterated cadmium arachidate film with a per-protonated topmost layer and (c), nine layer per-deuterated cadmium arachidate film with a per-protonated lowermost layer. All films were deposited on hydrophobic gold and the spectra recorded in the PPP beam polarization combination. Broken lines have been aligned with features of spectrum (a). Individual spectra in this and subsequent figures have been displaced vertically from each other for clarity.

substrates were employed, the sample was irradiated through the hemicylindrical side of the prism, and in this configuration the visible and SFG beams were totally internally reflected, leading to higher electric fields and consequently a larger SFG signal. On gold, the signal was intrinsically enhanced due to the high nonresonant susceptibility of the metal. Spectra were recorded in the PPP laser beam polarization combination for multilayers adsorbed on gold substrates and in the SSP laser beam polarization for multilayers adsorbed on a fused quartz prism. Integration times of 60 and 180 s were necessary on the gold and fused quartz substrates, respectively to achieve good signal-to-noise ratios. The spectra were fitted with Lorentzian line profiles using a Levenberg–Marquardt least-squares fitting routine.³⁴

Results and Discussion

(a) Spectra on Gold. Figure 1 presents broadband 800-nm excited femtosecond SFG spectra of three different cadmium arachidate multilayer films deposited on d-ODT modified gold substrates. Figure 1a is the spectrum of a 10-layer per-protonated film and contains resonances that are attributable to the terminal methyl groups (r) and the methylene groups (d) of the aliphatic chains of the arachidate anion. Specifically, the resonances may be assigned as follows: methyl symmetric stretch, r^+ at 2883 cm^{-1} , Fermi resonance of the methyl symmetric stretch, r_{FR}^+ at 2945 cm^{-1} , methyl asymmetric stretch, r^- at 2975 cm^{-1} , and methylene symmetric stretch, d^+ at 2857 cm^{-1} . The presence of the d^+ resonance in the spectrum indicates the existence of

gauche defects and hence a lack of centrosymmetry (giving rise to SFG activity) in the fatty acid hydrocarbon chains. This result is unexpected since fatty acid alkyl chains deposited under these conditions are typically close packed on a hydrophobic surface and hence exist in an all-trans conformation, as shown for example by previous SFG measurements on a comparable system using a 532-nm excited nanosecond laser system.²³ It is noted that the line shapes of the resonances of Figure 1a resemble first derivative in profile rather than consisting of peaks (phase $+90^\circ$) or dips (phase -90°). The interpretation of the spectral features in Figure 1 is considered below.

The authors' earlier investigation of multilayer films of cadmium arachidate deposited on comparable hydrophobic substrates employing a nanosecond spectrometer revealed via deuteration of selected layers that the SFG spectrum was composed of contributions solely from the topmost and lowermost fatty acid layers of the film.²³ A comparable experimental scheme has been employed in the present study to probe the origin of the 800-nm excited femtosecond SFG signal. Specifically, Figures 1b and 1c are femtosecond spectra of 10-layer films comprising nine layers of per-deuterated and one layer of per-protonated arachidate. Since the spectra are recorded in the C–H stretching region, it is solely the per-protonated layers that give rise to the resonant SFG signal. In Figure 1b the per-protonated layer is topmost in the film and in contact with air while in Figure 1c the per-protonated layer is lowermost and in contact with the hydrophobic gold substrate. In accordance with predictions of arachidate chain orientation based on the deposition cycle, the resonances appear with dips (negative phase) for methyl chain terminating groups oriented into air (Figure 1b) and with peaks (positive phase) for methyl groups oriented toward the substrate (Figure 1c). It is noted that a weak methylene resonance is present in Figure 1c but is absent in Figure 1b. This indicates the presence of gauche defects in the per-protonated arachidic acid layer in contact with the d-ODT covered gold substrate. These may arise from imperfections introduced into the film during sample preparation or from a mismatch in alkyl chain conformation between the covalently bound close packed structure of the d-ODT layer and the LB deposited arachidic acid film. No such interface exists for the per-protonated layer topmost in the film and exposed to air and as such no methylene resonance is observed in the corresponding spectrum (Figure 1b). It is also noted that a distinct red shift in resonance frequencies exists when comparing Figures 1c with 1b. The shift corresponds to a change in the local environment of the resonant groups and is consistent with results in linear spectroscopy³⁵ and previous SFG studies.²³

To substantiate the conclusion reached from the nanosecond SFG investigation of a multilayer film comprising solely per-protonated arachidate, namely that the SFG spectrum was due only to contributions from the topmost and lowermost layers,²³ a spectrum was generated via summation of the two single layer spectra of Figures 1b and 1c. This spectrum is shown in Figure 2a. The broadband femtosecond spectrum of a 10-layer fully per-protonated multilayer film of Figure 1a is reproduced as Figure 2b. Comparison of the spectra in Figure 2 reveals that the spectrum obtained by simple co-addition of the individual spectra of the topmost and lowermost layers is similar to the experimentally measured spectrum. It should be noted, however, that the intensity of 2a is lower than 2b. The reason for this is not clear but some structural changes may occur in these anisotropic films which may reduce the SFG intensity. Nevertheless, the result suggests that, in common with the nanosecond case, no significant contribution to the spectrum from arachidate

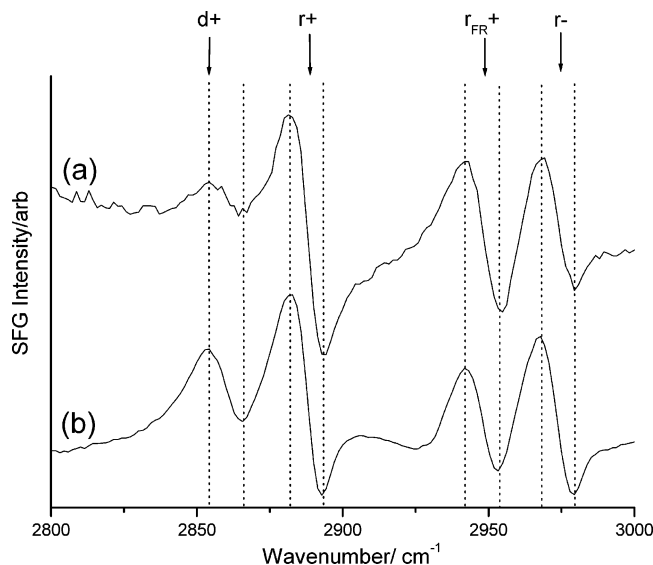


Figure 2. (a) Normalized spectrum obtained by numerical addition of the two single-layer SFG spectra of Figures 1b and 1c. (b) The experimental 10-layer per-protonated cadmium arachidate multilayer film reproduced from Figure 1a.

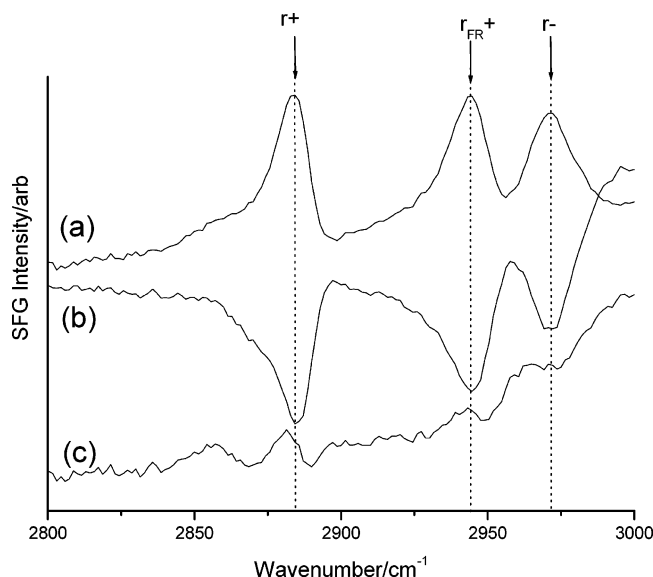


Figure 3. The 800-nm excited broadband SFG spectra of (a) nine-layer perdeuterated cadmium arachidate multilayer film with a perdeuterated layer at layer five, (b) nine-layer perdeuterated cadmium arachidate multilayer film with a per-protonated layer at layer two, and (c) the numerical addition of spectra (a) and (b).

layers within the structure exists. This finding may be qualitatively understood by considering the film to consist of a series of cadmium arachidate bilayers, each of which is SFG inactive due to the presence of a plane of symmetry between the layers. This hypothesis has been confirmed by comparing the spectra of two per-protonated layers buried within an otherwise perdeuterated film. Figures 3a and 3b present the 800-nm excited femtosecond spectra of single layers of per-protonated arachidate at layers 5 and 2, respectively, in a 10-layer film on hydrophobic gold. The phase of the resonances follows that expected for the opposite orientation of the individual layers within the film. Investigation of Figure 3 reveals that there is no shift in wavenumber between the spectra, indicative of the presence of the layers in a comparable environment and conformational state. The spectrum obtained via numerical addition of spectra 3a and 3b is presented as spectrum 3c. This spectrum is essentially

featureless, confirming the absence of SFG from the bulk of single isotope fatty acid films.

It is further instructive to compare the SFG spectra of the purely per-protonated multilayer spectra acquired on both spectrometers with the corresponding spectra of lowermost and topmost layers. While the nanosecond SFG spectrum of the isotopic multilayer has been shown to be mainly that of the topmost layer, albeit slightly modified by the lowermost layer, in contrast the femtosecond SFG spectrum of the isotopic multilayer appears to be substantially different from that of the topmost layer. Furthermore, the wavenumbers of the peaks and dips in the 800-nm excited isotopic multilayer spectra do not correspond to the wavenumbers of the peaks and dips in the lowermost and topmost layer spectra, respectively (Figure 1). Consequently interpreting this isotopic spectrum as being mainly that of the topmost layer is unjustified, as it can be seen to have a large contribution from the lowermost layer as shown in Figure 2.

There are several reasons for the differences between the isotopic multilayer spectra obtained from the two spectrometers, Figures 1 and 4. First, due to the co-propagating versus counter-propagating geometry of the 800-nm excited femtosecond spectrometer in relation to the 532-nm excited nanosecond spectrometer, the lowermost layer gives rise to peaks rather than dips in the spectrum from the former. It has been shown³⁶ that when the resonant and nonresonant contributions are of approximately the same magnitude, peak intensities are measurably larger than dip intensities for the same SFG resonance of a group oriented in opposite polar directions but in otherwise identical films. This is because on resonance the SFG intensity is now proportional to $|\chi_{NR}^{(2)} + \chi_R^{(2)}|^2$ rather than $|\chi_R^{(2)}|^2$. The former term, which contains the signed resonant susceptibility, $\chi_R^{(2)}$, determines the intensity of the SFG signal above or below the nonresonant background. The outcome is that the peak intensity (positive) may be higher above the background than the dip intensity (negative) will be below it. Hence a larger contribution from the lowermost layer to the overall spectrum occurs for the 800-nm excited femtosecond system. Second, the line width of the resonances observed in the femtosecond spectra are significantly broader than those of the nanosecond spectra, for example approximately 20 and 13 cm^{-1} (fwhm) respectively for the r^+ mode of the topmost layer spectra. The effect of line width on the isotopic multilayer spectra can be seen in the 532-nm excited nanosecond spectra of Figure 4. Most notably the r_{FR}^+ resonance of the lowermost layer and topmost layer spectra are comparatively broad and occur at significantly different wavenumbers (due to the difference in local environment of the resonant groups). Destructive interference of these two spectra leads to an apparent narrowing of the line width. A comparable but less dramatic effect is observed for the narrower r^+ resonance of Figure 4.

Finally, thin film interference effects arising from interaction between SF emission from the resonant topmost layer and the nonresonant gold substrate must be considered. Such effects have been previously observed in nanosecond SFG spectra of multilayer films on hydrophobic gold substrates and are manifest as a film thickness dependent change in phase of the r^- asymmetric methyl stretching mode with a periodicity of 162 nm.¹⁹ This effect is absent in the multilayer femtosecond spectra recorded in this and other studies.²² This observation is entirely explicable in terms of the thin film SFG interference model developed by Lambert et al.²⁷ There are four principal differences between the two SFG spectrometers, namely pulse length, laser line width, beam geometry, and wavelength. Only the last

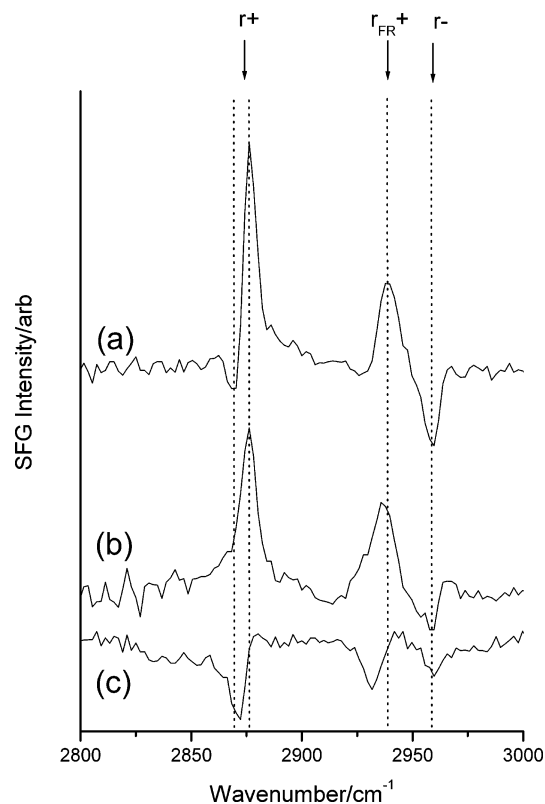


Figure 4. The 532-nm excited nanosecond SFG spectra of (a) ten-layer per-protonated cadmium arachidate multilayer film, (b) nine-layer per-deuterated cadmium arachidate film with a per-protonated topmost layer, and (c) nine-layer per-deuterated cadmium arachidate film with a per-protonated lowermost layer. All films were deposited on hydrophobic gold and the spectra recorded in the PPP beam polarization combination. Broken lines have been aligned with features of spectrum (a).

two factors are inherent in the Lambert et al. model, and their effects may be readily evaluated. A change in the input laser beam geometry does not affect the periodicity of the interference effect. On the other hand the interference effect is strongly dependent upon the wavelength of the incident beams employed. The femtosecond spectrometer employs 800 nm radiation, in contrast to the 532 nm wavelength of the nanosecond spectrometer. In the former case both the visible and SF beams have considerably longer wavelengths than the corresponding beams of the nanosecond spectrometer. The calculated periodicity of the nanoscale interference effect for the femtosecond spectrometer is consequently significantly longer than that of the nanosecond spectrometer, specifically, 258 nm versus 162 nm. This substantially greater periodicity will result in a much smaller phase change as the thickness varies. Indeed an interference effect was indiscernible in the r^- resonance for femtosecond spectra of up to twelve layers, the maximum thickness examined.

The relative complexity of the multilayer SFG spectra deposited on hydrophobic gold (Figures 1 and 4) contrast with the femtosecond spectra from multilayers deposited on (uncoated) hydrophilic gold substrates reported by Ye and co-workers.²² This finding is attributed to the fact that in the latter case (uncoated gold) only the methyl groups of the topmost layer are SFG active; all other methyl groups, including those in the lowermost layer in contact with the gold substrate, are located in bilayer environments, which are intrinsically centrosymmetric and for which SFG is symmetry forbidden. That is, multilayer films on hydrophilic gold in air have an odd number of layers with solely the topmost layer in a non-

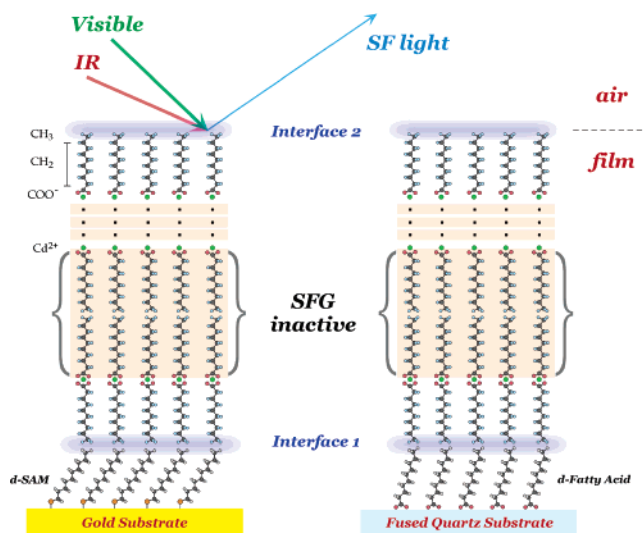


Figure 5. Schematic representation of cadmium arachidate fatty acid multilayer films deposited on deuterated SAM-modified gold and deuterated fatty acid covered fused quartz substrates indicating the two SFG active layers and the location of the SFG active functional groups at the relevant interfaces.

centrosymmetric environment oriented with its hydrophobic tail into air. Conversely, multilayer films on hydrophobic substrates in air consist of an even number of layers with the hydrophobic tail of the lowermost layer orientated toward the substrate in a noncentrosymmetric environment and the hydrophobic tail of the topmost layer oriented into air, also a noncentrosymmetric environment. Consequently, the observed SFG spectrum from a multilayer film on a hydrophobic substrate arises from a convolution of resonant SFG signals from two interfacial layers, rather than from a single interface as for films on hydrophilic substrates. Schematic representations of the different multilayer structures formed on d-ODT modified gold and d-arachidic acid modified fused quartz substrates are shown in Figure 5.

As anticipated by eq 8, the SFG signal arising from a multilayer system comprising two SFG active layers deposited on a gold substrate is contributed to by four terms. The contributions of the first two terms have been experimentally determined by measuring individual spectra of the topmost and lowermost layers on the substrate. Figures 1 and 2 demonstrate that a simple summation of these two spectra generally reproduces the shape of the measured isotopic SFG spectrum and hence infer that the third and fourth terms of eq 8 make negligible contributions. This finding may be understood through a simulation based on eq 8 employing typical spectral parameters obtained from fitting the SFG spectra of the individual layers on a gold substrate. The two dotted lines in Figure 6 correspond to the simulated SFG spectra for the topmost and lowermost layers of a 10-layer system on a hydrophobic gold substrate. As discussed above, the observation of reversed phases is a result of the opposite orientations of the two layers, while the red shift of the resonance peaks for the lowermost layer is a consequence of the difference in chemical environment. The methylene resonances resulting from gauche defects in the experimental spectra were not modeled for the sake of clarity. The relative magnitude of $|\chi_{NR}^{(2)}|^2$ in these spectra is approximately 0.25 a.u., of the same order of magnitude as $|\chi_R^{(2)}|^2$. As a result, the peak intensities (positive) are higher above the background than the dip intensities (negative) are below it, as rationalized earlier.

The blue line in Figure 6 represents the simulated spectrum obtained via application of eq 8 and employing the fitting parameters discussed above. The red line in Figure 6 represents

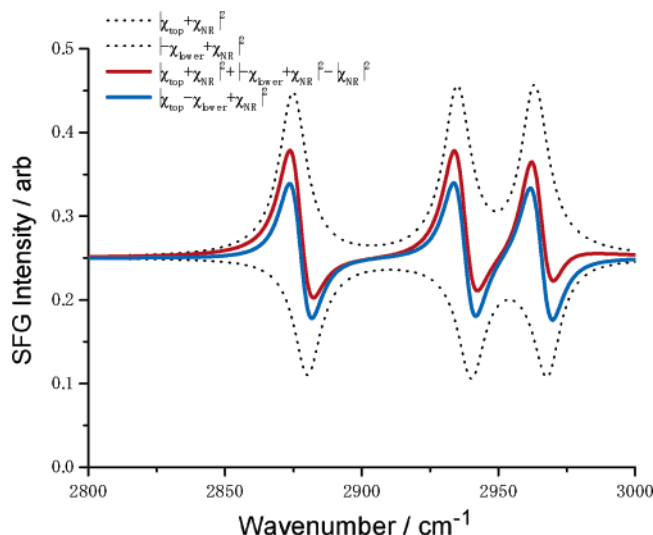


Figure 6. Simulated SFG spectra, shown by dotted lines, of the topmost and lowermost layers of a 10-layer film on a hydrophobic gold substrate. The red line corresponds to the numerical summation of the two individually fitted spectra. The blue line represents the simulated spectrum obtained via application of eq 8 employing the parameters derived from the fitting of the topmost and lowermost layer spectra (dotted lines).

the numerical summation of the two individual spectra given by the two dotted lines. Although minor differences in relative intensity exist between the blue and red simulated spectra, the two profiles are remarkably similar. It is concluded that the third and fourth terms of eq 8 make only a minor contribution and consequently that a simple summation of the two individual spectra of the topmost and lowermost layers may be used as an acceptable approximation for isotopic layers on the hydrophobic gold surface.

(b) Spectra on Fused Quartz. We now turn our attention to the SFG spectra of cadmium arachidate multilayer films on dielectric surfaces, specifically fused quartz, recorded with the 800 nm femtosecond laser system. The nonresonant susceptibility of fused quartz is insignificant in comparison to that of metals such as gold. As such, the amplification of the SFG signal via the cross term of eq 2 is nearly absent. Due to the lower E-fields produced by nanosecond laser spectrometers and their consequent lower sensitivity, pico- or femtosecond spectrometers are therefore typically required for the investigation of such systems. In the absence of a nonresonant susceptibility contribution to the SFG spectrum of species on dielectric substrates, an additional consequence is that the phase difference between the resonant and nonresonant terms of eq 2 disappears and hence molecular orientation information derived from the phase of the resonant line shape may not be obtained. However, on dielectric substrates, such as fused quartz, multiple beam polarization combinations may be effectively employed to probe specific components of the resonant susceptibility tensor (for example the SSP beam polarization combination which probes solely the $\chi_{yyz}^{(2)}$ component) and hence quantify adsorbate tilt angles. Such a methodology is not feasible on gold, for which a single beam polarization combination, PPP, is most commonly employed.

Figure 7 presents SSP beam polarization combination SFG spectra of three different cadmium arachidate multilayer films deposited on hydrophobic fused quartz substrates. The native hydrophilic surface of the substrates was first made hydrophobic via LB deposition of a single layer of per-deuterated cadmium arachidate in a manner analogous to the d-ODT treatment of gold to produce hydrophobic gold substrates. Figure 7a is the

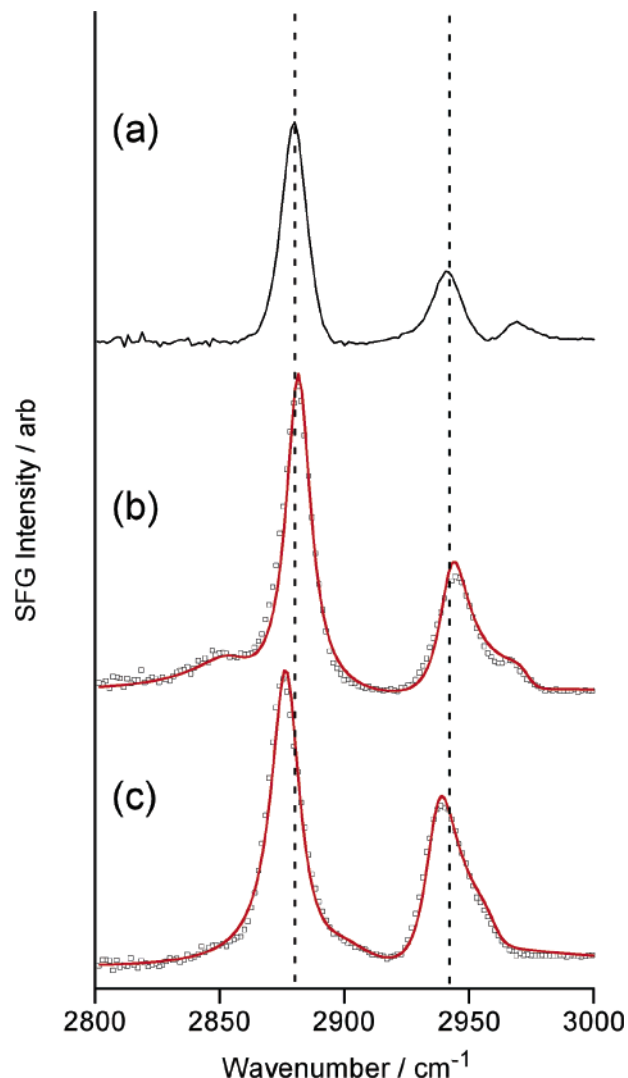


Figure 7. The 800-nm excited broadband SFG spectra of: (a) ten-layer per-protonated cadmium arachidate multilayer film, (b) nine-layer per-deuterated cadmium arachidate film with a per-protonated topmost layer, and (c) nine-layer per-deuterated cadmium arachidate film with a per-protonated lowermost layer. All films were deposited on hydrophobic fused quartz and the spectra recorded in the SSP beam polarization combination. Open squares represent experimental points and the red solid lines are fits to the spectra (Figure 7(b) and 7(c)) obtained as described in the Experimental Section.

spectrum obtained from a 10-layer per-protonated film deposited on hydrophobic fused quartz. The spectrum is considerably simpler than the corresponding spectrum on hydrophobic gold, Figure 1a. Specifically, the spectrum of Figure 7a contains solely resonances attributable to methyl modes. No methylene resonances, such as the d^+ resonance of Figure 1a, are observed. The superficial conclusion from examination of Figure 7a would be that the SFG active layer (or layers) of the multilayer film is highly ordered and in a predominantly all-trans conformation. However, as discussed below, this conclusion may not be definitively reached without examination of the component spectra. Further, it is noted that, in contrast to the derivative shaped line profiles of Figure 1a, the resonances of Figure 7a occur, as expected, as spectral peaks (that is with a phase of $\sim 90^\circ$). An additional reason for the apparent simplicity of Figure 7a relative to Figure 1a is that it has been recorded in the SSP, rather than the PPP beam polarization combination. As such only a single resonant susceptibility component ($\chi_{yyz}^{(2)}$) has been sampled.

Figure 7b shows the spectrum from a multilayer film comprising the lower nine cadmium arachidate layers per-deuterated and the topmost layer (in contact with air) per-protonated. Although superficially similar, there are differences between the spectra of Figures 7a and 7b. Specifically, the line widths of the resonances of the fully per-protonated film, 7a, are smaller than those of the film consisting of a single per-protonated topmost layer, 7b, 11 cm^{-1} versus 14 cm^{-1} (fwhm). In addition, while the spectrum of the fully per-protonated 10-layer film shows a distinct and well resolved methyl asymmetric stretching mode (r^-) resonance, it is not resolved in the spectrum of Figure 7b and occurs as a shoulder on the high wavenumber side of the Fermi resonance of the methyl symmetric stretch, r_{FR}^+ . Further, it is noted that there is a weak d^+ methylene symmetric stretch present in Figure 7b at $\sim 2850\text{ cm}^{-1}$ that is absent in the spectrum of Figure 7a. The appearance of this resonance is indicative of a small degree of conformational disorder in the per-protonated layer and is likely due to slightly imperfect film formation for this particular sample. The spectrum in Figure 7c is that recorded from a 10-layer cadmium arachidate film comprising a per-protonated lowermost layer in contact with the hydrophobic fused quartz substrate with the remaining nine upper layers per-deuterated. Comparison of the spectrum in Figure 7c with those in 7a and 7b reveals that the resonances of the single per-protonated lowermost layer film (Figure 7c) are red shifted by approximately 5 cm^{-1} , a fact explicable in terms of the different chemical environment of the alkyl chains in the lowermost and topmost layers, see above. In contrast with Figures 7a and 7b, the only evidence for the asymmetric methyl stretching resonance in Figure 7c is the weak shoulder on the Fermi resonance feature. It is noted that unlike the corresponding spectrum on a hydrophobic gold substrate (Figure 1c), no methylene symmetric stretching mode is observed in Figure 7c. This observation is attributed to the fact that, unlike in the hydrophobic gold system where the lowermost cadmium arachidate layer is in contact with an alkanethiol with a different surface density and tilt angle, in the fused quartz system the substrate is made hydrophobic via deposition of a layer of cadmium arachidate. As such, no mismatch in surface density and tilt angle (normal to the interface) between the hydrophobic substrate and the lowermost layer exists.

The topmost and lowermost spectra shown in Figures 7b and 7c, respectively, may be employed to calculate a predicted spectrum of a fully per-protonated multilayer film via eq 6. To facilitate the use of eq 6, each resonance of the spectra of Figures 7b and 7c must first be fitted to eq 7, as outlined in the Theory section. The parameters resulting from this procedure are given in Table 1. The predicted fully per-protonated multilayer film spectrum calculated via this methodology is presented in Figure 8, overlaid on the experimental fully per-protonated multilayer film spectrum of Figure 7a. Clearly the predicted spectrum correlates well with the experimental data and captures many of the salient features, although some minor differences, for example the relative intensity of the r^- resonance, do exist. Importantly, the wavenumber of the r^+ resonance is correctly reproduced, as is its decreased line width in comparison to the individual layer spectra. Similarly, the wavenumber and line width of the r_{FR}^+ resonance are accurately predicted. Finally, a well-resolved r^- resonance is generated, in comparison to the individual layer spectra, in which it is either present as a shoulder on the r_{FR}^+ mode, or absent. The observation of narrower r^+ and r_{FR}^+ resonances and a well resolved r^- resonance stems from the fact that the isotopic multilayer spectrum arises from interference between the individual topmost and lowermost

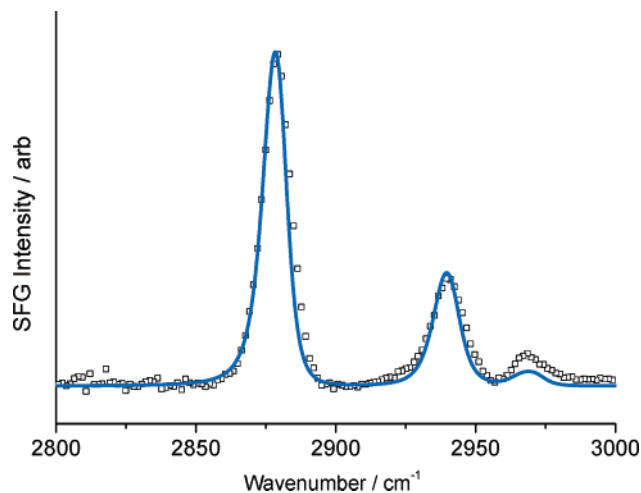


Figure 8. The 800-nm excited broadband SFG spectrum of a 10-layer per-protonated cadmium arachidate multilayer film on hydrophobic fused quartz reproduced from Figure 7a, open squares. Simulated SFG spectrum calculated via eq 6, employing fitting parameters for the spectra of Figures 7b and 7c, as presented in Table 1, solid line. The intensity of the simulated SFG spectrum was normalized to the peak intensity of the CH_3 symmetric stretching mode.

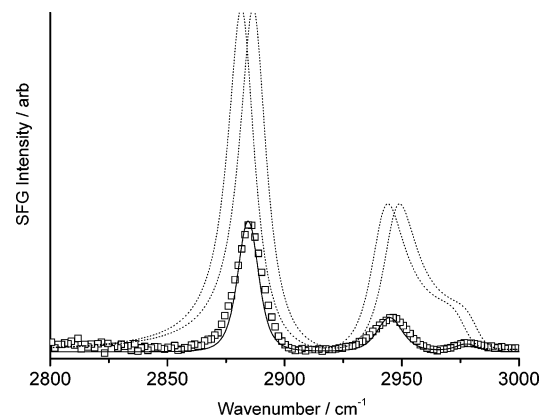


Figure 9. The 800-nm excited broadband SFG spectrum of an eight-layer per-deuterated cadmium arachidate multilayer film with per-protonated topmost and lowermost layers, open squares. Simulated SFG spectrum (solid line) obtained by application of eq 6 to two theoretical SFG spectra for the topmost and lowermost cadmium arachidate layers (broken lines). The theoretical spectra were generated such that the resonances in both layers were identical in magnitude but opposite in phase and with resonance frequencies shifted by 5 cm^{-1} .

TABLE 1: Parameters Acquired by Fitting the Spectra in Figures 7b and 7c to Equation 7

	topmost layer			lowermost layer		
	ω_v (cm^{-1})	Γ (cm^{-1})	A	ω_v (cm^{-1})	Γ (cm^{-1})	A
r^+ resonance	2881	6.00	0.67	2876	7.00	0.76
r_{FR}^+ resonance	2942	7.30	0.52	2937	8.00	0.60
r^- resonance	2973	6.00	-0.10	2963	8.00	-0.10

spectra (as per eq 6), which are offset from each other in frequency (Figures 7b and 7c).

To demonstrate conclusively that the SFG spectrum of an isotopic multilayer film adsorbed on a dielectric substrate arises solely from interference between SFG from the lowermost and topmost layers, a multilayer film was created with per-protonated lowermost and topmost layers separated by eight per-deuterated cadmium arachidate layers. Figure 9 presents the SFG spectrum (open squares) recorded from this film. In accordance with prediction the spectrum is virtually identical to that of the

experimental isotopic multilayer (Figure 7a). The solid line of Figure 9 represents a simulated spectrum calculated via eq 6 from two theoretical SFG spectra for the topmost and lowermost cadmium arachidate layers (broken lines). The theoretical spectra were generated such that the resonances in both layers were identical in magnitude but opposite in phase and with resonance frequencies shifted by 5 cm^{-1} . The quality of the fit demonstrates the utility of eq 6 in predicting the SFG spectra of multilayer films on dielectric substrates.

Conclusion

SFG spectra of cadmium arachidate multilayer films deposited on hydrophobic gold and fused quartz substrates have been measured and analyzed. It has been shown that in both cases the SFG signal arises solely from the topmost and lowermost layers. However, the relative contributions of these layers to the spectra are dependent upon the laser beam geometry and the nature of the substrate. The fact that the measured SFG spectrum is a convolution of the individual spectra of the lowermost and topmost layers is clearly evident on hydrophobic gold substrates. However, it is far less evident and subtler in the apparently much simpler spectra on fused quartz substrates. It has been demonstrated that the observed substrate-related spectral differences can be explained, and successfully modeled, in terms of the relative nonresonant strengths of fused quartz and gold. Further, two forms of spectral interference have been shown to occur in the spectra of thin films: first, that between the two resonantly active layers of the film, which depends on the spectral overlap of the two films and their spatial displacement; and second, in the case of gold substrates, an interference arising from the gold substrate and the spatially displaced resonant topmost SFG active layer of the film.

The current work has laid the foundations for understanding how the optical properties of the substrate, in particular its non resonant susceptibility, can combine with the resonant susceptibility of two SFG active molecular layers to influence the appearance of the SFG spectrum. In the work described in this article, the methyl groups, which are SFG active in the organic molecular layers have opposite polar orientation because they are the topmost and lowermost layers of an even-numbered film as depicted in Figure 5. It is interesting to speculate here on how the analytical method presented in the theory section may be developed to describe the SFG spectra arising from two or more SFG active layers in a multilayer film in which these layers have the same, rather than opposite, polar orientation. Experimentally, such a film can be formed by per-protonating every other layer in a per-deuterated film. Such experiments are currently under way.

Given the breadth of the potential applications and the rapid expansion of SFG spectroscopy to thin films consisting of polymers, surfactants, and fatty acid (LB) multilayers, the outcome of the present study shows that it is essential that researchers in the field recognize the potential complexity and origins of the recorded spectra. By recognizing the importance of the substrate and of experimental parameters such as the film thickness, beam geometry, and excitation wavelength, it is possible to unambiguously interpret the SFG spectra of thin films composed of multilayers in which there may be several sources of sum frequency generation.

Acknowledgment. We are grateful to the Leverhulme Trust for financial support through Research Grant F/09/650/A, and the Oppenheimer Fund of the University of Cambridge for a studentship for J.H. We also gratefully acknowledge visiting Fellowships from the Japan Society for the Promotion of Science

(JSPS) to J.H. and P.B.D. to enable them to carry out experimental work at Hokkaido University. Per-deuterated arachidic acid was kindly provided by the Port Sunlight Laboratory of Unilever Research and Development. S.Y. gratefully acknowledges support from PRESTO, the Japan Science and Technology Corporation (JST), the Akiyama Foundation, and the Nippon Sheet Glass Foundation for Materials Science and Engineering.

References and Notes

- (1) *An introduction to ultrathin organic films from Langmuir–Blodgett to self-assembly*; Ulman, A., Ed.; Academic Press: San Diego, CA 1991.
- (2) Peng, J. B.; Barnes, G. T.; Gentle, I. R. *Advances in Colloid and Interface Sci.* **2001**, *91*, 163–219.
- (3) *Nanoparticles and Nanostructured Films*; Fendler, J. H., Ed.; Wiley-VCH: Weinheim, 1998.
- (4) Adamson, A. W.; Gast, A. P. *Physical Chemistry of Surfaces*, 6th ed.; Wiley-Interscience: New York, 1997.
- (5) Smotkin, E. S.; Lee, C.; Bard, A. J.; Campion, A.; Fox, M. A.; Mallouk, T. E.; Webber, S. E.; White, J. M. *Chem. Phys. Lett.* **1988**, *152*, 265–268.
- (6) Foran, G. J.; Peng, J. B.; Steitz, R.; Barnes, G. T.; Gentle, I. R. *Langmuir* **1996**, *12*, 774–777.
- (7) Russell, G. J.; Petty, M. C.; Peterson, I. R.; Roberts, G. G.; Lloyd, J. P.; Kan, K. K. *J. Mater. Sci. Lett.* **1984**, *3*, 25–28.
- (8) Schwartz, D. K.; Garnas, J.; Viswanathan, R.; Zasadzinski, J. A. *N. Science* **1992**, *257*, 508–511.
- (9) Florsheimer, M.; Steinfort, A. J.; Gunter, P. *Surf. Sci.* **1993**, *297*, L39–L42.
- (10) *The Principles of Nonlinear Optics*; Shen, Y. R., Ed.; John Wiley & Sons: New York, 1984.
- (11) Harris, A. L.; Chidsey, C. E. D.; Levinos, N. J.; Loiacono, D. N. *Chem. Phys. Lett.* **1987**, *141*, 350–356.
- (12) Ward, R. N.; Davies, P. B.; Bain, C. D. *J. Phys. Chem.* **1993**, *97*, 7141–7143.
- (13) Beattie, D. A.; Bain, C. D. In *Handbook of Vibrational Spectroscopy*; Chalmers, J. M.; Griffiths, P. R., Eds.; John Wiley & Sons Ltd.: Chichester, 2002; pp 801–811.
- (14) Ye, S.; Uosaki, K. In *Encyclopedia of Electrochemistry*; Bard, A. J., Ed.; Wiley-VCH: Weinheim, 2005; Vol. 10, in press.
- (15) Richter, L. J.; Petralli-Mallow, T. P.; Stephenson, J. C. *Optics Lett.* **1998**, *23*, 1594–1596.
- (16) Zhang, D.; Ward, R. S.; Shen, Y. R.; Somorjai, G. A., *J. Phys. Chem. B* **1997**, *101*, 9060–9064.
- (17) Liu, J.; Conboy, J. C. *J. Am. Chem. Soc.* **2004**, *126*, 8376–8377.
- (18) Li, G.; Ye, S.; Morita, S.; Nishida, T.; Osawa, M. *J. Am. Chem. Soc.* **2004**, *126*, 12198–12199.
- (19) McGall, S. J.; Davies, P. B.; Neivandt, D. J. *J. Phys. Chem. B* **2004**, *108*, 16030–16039.
- (20) Chen, Z.; Shen, Y. R.; Somorjai, G. A. *Annu. Rev. Phys. Chem.* **2002**, *53*, 437–465.
- (21) Ye, S.; Morita, S.; Li, G.; Noda, H.; Tanaka, M.; Uosaki, K.; Osawa, M. *Macromolecules* **2003**, *36*, 5694–5703.
- (22) Ye, S.; Noda, H.; Morita, S.; Uosaki, K.; Osawa, M. *Langmuir* **2003**, *19*, 2238–2242.
- (23) Holman, J.; Davies, P. B.; Neivandt, D. J. *J. Phys. Chem. B* **2004**, *108*, 1396–1404.
- (24) Holman, J.; Ye, S.; Neivandt, D. J.; Davies, P. B. *J. Am. Chem. Soc.* **2004**, *126*, 14322–14323.
- (25) Ye, S.; Noda, H.; Nishida, T.; Morita, S.; Osawa, M. *Langmuir* **2004**, *20*, 357–365.
- (26) Holman, J.; Neivandt, D. J.; Davies, P. B. *Chem. Phys. Lett.* **2004**, *386*, 60–64.
- (27) Lambert, A. G.; Neivandt, D. J.; Briggs, A. M.; Usadi, E. W.; Davies, P. B. *J. Phys. Chem. B* **2002**, *106*, 5461–5469.
- (28) Bain, C. D.; Davies, P. B.; Ong, T. H.; Ward, R. N.; Brown, M. A. *Langmuir* **1991**, *7*, 1563–1566.
- (29) Potterton, E. A.; Bain, C. D. *J. Electroanal. Chem.* **1996**, *409*, 109–114.
- (30) Hines, M. A.; Todd, J. A.; Guyot-Sionnest, P. *Langmuir* **1995**, *11*, 493–497.
- (31) Ishibashi, T.; Onishi, H. *Appl. Phys. Lett.* **2002**, *81*, 1338–1340.
- (32) Bain, C. D. *J. Chem. Soc., Faraday Trans.* **1995**, *91*, 1281–1296.
- (33) Briggs, A. M.; Johal, M. S.; Davies, P. B.; Cooke, D. J. *Langmuir* **1999**, *15*, 1817–1828.
- (34) Ye, S.; Nihonyanagi, S.; Uosaki, K. *Phys. Chem. Chem. Phys.* **2001**, *3*, 3463–3469.
- (35) Cameron, D. G.; His, S. C.; Umemura, J.; Mantsch, H. H. *Can. J. Chem.* **1981**, *59*, 1357–1360.
- (36) Holman, J.; Ph.D. Thesis; University of Cambridge, Cambridge, UK 2005.